Kinetic Study to Predict Sigma Phase Formation in Duplex Stainless Steels

DANIELLA CALUSCIO DOS SANTOS and RODRIGO MAGNABOSCO

This work presents an improved kinetic study of sigma phase formation during isothermal aging between 973 K and 1223 K (700 °C and 950 °C), based on Kolmogorov-Johnson-Mehl-Avrami (K-J-M-A) model, established from volume fraction of sigma phase determined in backscattered electron images over polished surfaces of aged samples. The kinetic study shows a change in the main mechanism of sigma formation between 973 K and 1173 K (700 °C and 900 °C), from a nucleation-governed stage to a diffusion-controlled growth-coarsening stage, confirmed by a double inclination in K-J-M-A plots and microstructural observations. A single inclination in K-J-M-A plots was observed for the 1223 K (950 °C) aging temperature, showing that kinetic behavior in this temperature is only related to diffusion-controlled growth of sigma phase. The estimated activation energies for the nucleation of sigma phase are close to the molybdenum diffusion in ferrite, probably the controlling mechanism of sigma phase nucleation. The proposed time-temperature-transformation (TTT) diagram shows a "double c curve" configuration, probably associated to the presence of chi-phase formed between 973 K and 1073 K (700 °C and 800 °C), which acts as heterogeneous nuclei for sigma phase formation in low aging temperatures.

I. INTRODUCTION

THE industrial interest in materials that possess high mechanical and corrosion resistance led to the development of duplex stainless steels (DSS). These steels are widely used in the chemical equipment, oil and gas industry, desalinization plants, pollution control and most recently in off-shore applications like oil extraction in deep water.[1] DSS are composed of ferrite (α) and austenite (γ) in approximately equal amounts and the high amounts of Cr, Mo, and N ensure high corrosion resistance.[2,3]

Nevertheless, the exposure of DSS to temperatures between 873 K and 1273 K (600 °C and 1000 °C) will induce the formation of intermetallic phases, such as sigma (σ) and chi (χ), and also chromium nitrides (Cr_2N).[2–7] Sigma is brittle, rich in Cr and Mo, and its formation reduces corrosion resistance and toughness,[2–9] in the same manner as chi-phase, which is richer in Mo than sigma. Other studies suggest that chi acts as heterogeneous nuclei for sigma phase formation.[1–3,5,10] Chromium nitrides may be present in these steels and can be formed during aging or during quenching from solution-treatment temperature.[3–5] Nevertheless, both chi and chromium nitrides are

formed in lower volume fractions if compared to sigma phase.

The proposed mechanisms of sigma phase formation are[3–5,7,11,12]:

a. Continuous or discontinuous precipitation from ferrite ($\alpha \rightarrow \sigma + \alpha_2$);
b. Eutectoid decomposition of ferrite ($\alpha \rightarrow \sigma + \gamma_2$);
c. Sigma formation from austenite ($\gamma \rightarrow \sigma + \gamma_2$).

All the mechanisms generate Cr- and Mo-depleted secondary phases (secondary austenite—γ_2, or secondary ferrite—α_2), reducing the corrosion resistance of DSS, particularly reducing pitting corrosion resistance.[6] It is important to emphasize that both discontinuous precipitation and eutectoid decomposition of ferrite leads to sigma formation with a lamellar morphology, which makes the prediction of the main mechanism for sigma phase formation from microstructural characterization even more complex.[4,5,7,8]

The kinetics of sigma phase formation can be described by the K-J-M-A (Kolgomorov-Johnson-Mehl-Avrami) model, presented in Eq. [1][13–18]:

$$f = 1 - e^{(-k \cdot t^n)}, \qquad [1]$$

where f ($0 < f < 1$) is the sigma fraction, k is a constant related to the activation energy to sigma phase formation, t is the transformation time, and n is the K-J-M-A exponent, related to the nucleation and/or growth mechanism of sigma formation. Usually when n is between 1 and 4, the transformation process can be related to interface controlled nucleation and growth; when the same exponent is between 0.5 and 2.5, the growth could be controlled mainly by diffusion.[19]

DANIELLA CALUSCIO DOS SANTOS, Assistant Professor, and RODRIGO MAGNABOSCO, Professor, are with the Ignatian Educational Foundation (FEI), Av. Humberto Castelo Branco, 3972, São Bernardo do Campo, SP 09850-901, Brazil. Contact e-mail: dcaluscio@fei.edu.br

Between 1 and 2.5, all the mechanisms can occur concomitantly.

The constant k depends on the number of formed nuclei and on the growth rate of particles and is described by Eq. [2]:

$$k = k_0 \cdot e^{\left(-\frac{Q_\sigma}{RT}\right)}, \qquad [2]$$

where k_0 is a pre-exponential constant, Q_σ is the activation energy for sigma phase formation, T is the absolute temperature and R is the gas universal constant, considering that Q_σ is proportional to 1 mol of alloy.

The kinetic study of sigma phase formation were explored earlier,[7,11,17] and a divergence between proposed kinetic mechanisms was observed. Palmer et al.[17] suggested that a change in the mechanism of sigma phase formation occurs during aging. The authors mentioned that in the beginning of aging time, n varies between 7 for high and 0.75 for low temperatures and sigma was formed by continuous precipitation controlled by interface. With increasing aging time, the mechanism changes to a diffusion-controlled growth.[19]

However, Magnabosco[11] pointed that the mechanism of sigma phase formation is diffusion-controlled growth, with n values of approximately 0.9, during aging between 973 K and 1123 K (700 °C and 850 °C), and proposed that the activation energy for sigma phase formation may be related to the activation energy for Cr diffusion in ferrite (185 kJ mol^{-1}).

Electron backscatter diffraction (EBSD) was used in a recent work[20] in order to study the kinetics of sigma phase formation. The authors worked with as received material, aged at 1073 K (800 °C) up to 100 hours, and chi was not detected through this technique. Even though the authors have selected $n = 1$ based on the shape of the sigmoidal curve, and a fewer points have been considered if compared to the other works previously reported,[11,17,18] a single slope in the K-J-M-A plots was registered.

In a previous exploratory investigation,[7] we found that at 1123 K (850 °C), the n exponent could vary from 1.57 in the early stages of sigma phase formation to 0.67. This indicates that the main mechanism of sigma phase formation was the nucleation and growth from ferrite. However, there is possibly a change on the mechanism of sigma phase formation from nucleation and growth from ferrite (early stages) to the growth from austenite with increasing aging time, as suggested by the double slope on K-J-M-A plots for 1123 K (850 °C).

The purpose of this paper is to present an improved kinetic study based on K-J-M-A model of sigma phase formation between 973 K and 1223 K (700 °C and 950 °C). The novelty of the proposed work relies on the technique used to determine the volume fraction of sigma. In previous works,[7,11,17] sigma fraction was determined using optical microscopy after selective etching of intermetallic phases. Thus, the chi-phase was also etched and there is relief formation between phases; those occurrences decrease the accuracy in the measurement of sigma volume fraction. Using for the quantification of sigma and chi-volume fractions backscattered electron images (BSC), obtained by scanning electron microscopy (SEM) over polished surfaces, a better microstructural characterization of the sigma phase formation is achieved. More importantly, the better accuracy in determining sigma volume fraction resulted in a more accurate kinetic model based in K-J-M-A theory.

II. EXPERIMENTAL PROCEDURES

A UNS S31803 duplex stainless steel was used for the evaluation of the kinetic model. The chemical composition of the studied material is given in Table I. Samples were obtained from 3-mm thickness sheet. Solution heat treatment was conducted at 1448 K (1175 °C) for 30 minutes followed by water quenching, in order to obtain a duplex structure of ferrite and austenite.

After the solution heat treatment, samples were isothermally aged between 973 K and 1223 K (700 °C and 950 °C). The aging treatments were conducted between 1 minute to 360 hours. Aging between 1 and 5 minutes were possible using an aluminum bath in a muffle furnace to ensure efficient heat transfer to the sample. For the samples aged between 10 minutes and 360 hours, a vacuum tubular electric furnace was used, ensuring a nitrogen atmosphere to avoid excessive oxidation of the samples and preventing nitrogen loss from the material. Both aging treatments were interrupted by water quenching.

After heat treatments, specimens were abraded using silicon carbide (SiC) papers to a 220-grit finish before mounting in thermosetting plastic, parallel to the rolling direction. The mounted specimens were metallographic polished in a semi-automatic grounding and polishing machine, with final polishing provided by 0.25 μm diamond abrasive.

Solution-treated sample was observed by optical microscopy (OM) after two different etching procedures: modified Beraha reagent composed of 20 mL hydrochloric acid (HCl) and 80 mL distilled water, and to this stock solution, 1 g potassium metabisulphide ($K_2S_2O_5$) and 2 g of ammonium bifluoride ($NH_4F \cdot HF$) were added just before the etching, for differentiation between ferrite and austenite. Etching of grain boundaries and ferrite-austenite interfaces was obtained through electrolytic etching in 10 pct oxalic acid ($H_2C_2O_4$) aqueous solution (6 Vdc during 10 seconds).

All polished metallographic samples were examined in a CAMSCAN CS32000LV scanning electron microscopy through backscattered electron image (BSC), obtaining five images from each sample. Images were analyzed with the software OLYMPUS AnalySIS for the determination of the sigma (σ) and chi (χ)-volume fractions using quantitative stereology, assuming that the area fraction of each phase can be directly related to volume fraction. This analysis was based on grayscale differentiation of the phases. To achieve the differentiation between phases the electron microscopy adjustments were standardized for all samples (accelerating voltage applied to the electron beam was maintained at 20 kV, current emitted by the filament was maintained

Table I. Chemical Composition (wt pct) of the Studied Material									
Cr	Ni	Mo	Mn	N	C	Si	Cu	V	Fe
22.07	5.68	3.20	1.38	0.17	0.017	0.34	0.15	0.13	bal.

at 100 μA, working distance was kept at 20 mm, and brightness and contrast levels were the same for all images taken). These adjustments ensured that the shade and outline of the phases are the same at all collected images, avoiding differences in identification, and quantification of the phases.

Ferrite content (α) of the samples was obtained through magnetic measurements using a ferritscope (20 measurements were taken in each sample).

X-ray diffraction patterns (XRD) were also performed for phase characterization, using Cu-Kα radiation (wavelength of 0.154056 nm), acceleration potential of 30 kV, and filament current of 30 mA, at a scan rate of 1 deg/min and scan step of 0.04 deg.

III. RESULTS AND DISCUSSION

A. Microstructural Characterization

The solution treatment of UNS S31803 duplex stainless steel resulted in a sample composed only by ferrite and austenite as presented in Figure 1. In Figure 1(a), the solution-treated sample was etched using modified Beraha's reagent, being ferrite phase represented by black areas, while austenite appears as the light-gray areas. Figure 1(b) shows the same sample, electrolytic etched using oxalic acid at 6 Vcc for 10 seconds, revealing grain boundaries, interfaces between ferrite and austenite, and twin boundaries inside austenite grains. Magnetic measurement performed with the aid of a ferritscope shows that the solution-treated sample presents 57.3 ± 2.3 pct of ferrite.

Figure 2 presents the microstructural transformations of a sample that was subjected, after solution treatment, to isothermal aging at 973 K (700 °C). In the beginning of the aging treatment, a brighter phase decorates the ferrite/ferrite and ferrite/austenite boundaries (Figure 2a) followed by the preferential growth of this phase over ferrite as shown in Figures 2(b) through (d). Those brighter phases are probably sigma (σ) or chi (χ) phases, as will be discussed in the following paragraphs.

X-ray diffraction (XRD) patterns of the solution-treated sample and of the sample aged for 4 hours at 1023 K (750 °C), representative of the aged conditions studied here, are presented in Figure 3, together to typical BSC-SEM micrographs of both conditions. XRD of all aged conditions indicated the same trend of Figure 3(b): the presence of not only ferrite (α) and austenite (γ), but also the presence of sigma (σ) and chi (χ)-phases, and hexagonal close-packed (HCP) chromium nitrides (Cr$_2$N).

Similar microstructural characteristics were found in the other investigated aging temperatures, as presented in Figure 4. However, higher aging temperatures led to different morphologies of the brighter phases: a more
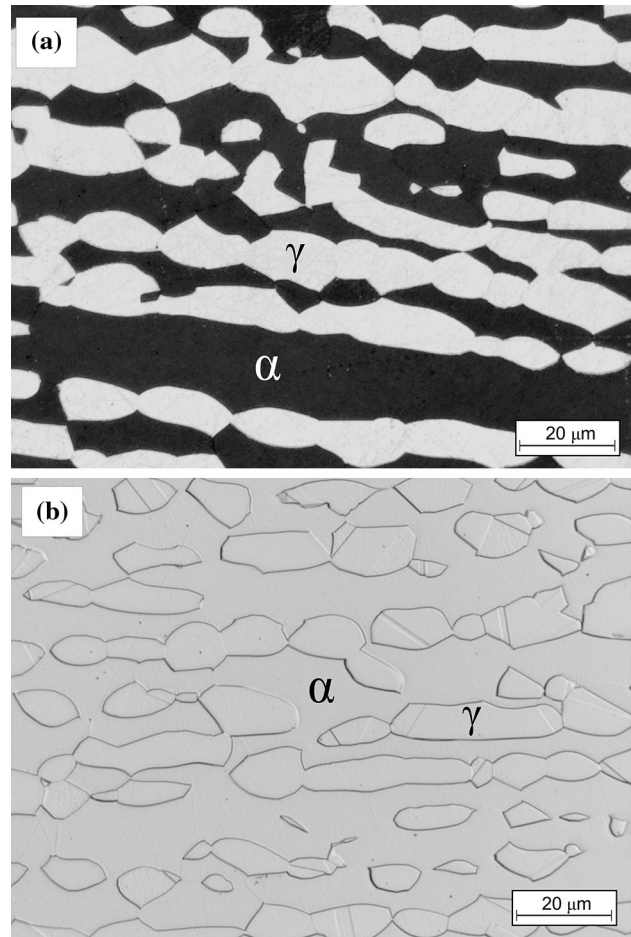

Fig. 1—UNS S31803 steel solution treated for 30 min at 1448 K (1175 °C), showing ferrite (α) and austenite (γ) phases (a) Beraha's etching; (b) eletrolytic oxalic acid etching.

compact morphology (Figure 4d) is observed in higher temperatures, while a lamellar morphology is observed in lower temperatures (Figures 4(a) through (c)).

The presence of sigma phase and Cr$_2$N is evident from the XRD analysis; however, chi-phase diffraction peaks are coincident with Cr$_2$N or σ phase peaks. Cr$_2$N are probably the darks spots in BSC images of Figures 2, 3(b), and 4(a) through (c), since Cr and N have atomic numbers lower than Fe, Mo, and Ni, the major components of the alloy. For that reason, the backscatter coefficient of Cr$_2$N is smaller than the one found in other phases, and the BSC image of Cr$_2$N areas will appear dark.[21] Nonetheless, another characterization method was required to differentiate sigma (σ) and chi (χ)-phases.

Considering that it is almost impossible to differentiate sigma and chi using the described techniques, especially in the earlier stages of aging considering the
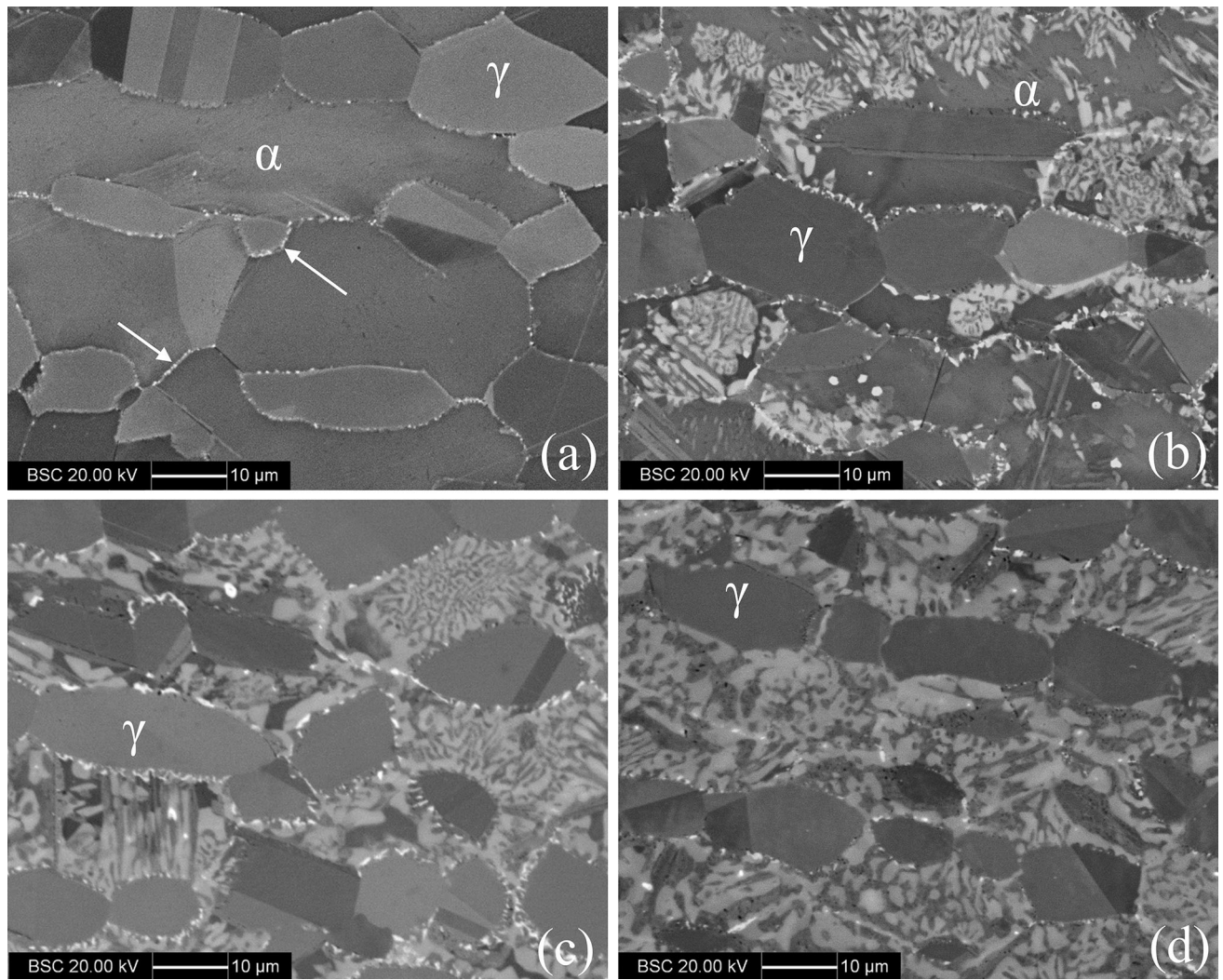
Fig. 2—Microstructures of UNS S31803 aged at 973 K (700 °C) for: (*a*) 2 h; (*b*) 6 h; (*c*) 36 h; and (*d*) 360 h. BSC-SEM images.

low volume fraction of sigma and/or chi (lower than 5 pct volume fraction), energy dispersive spectroscopy (EDS) analysis were performed in selected-aged samples. The chemical composition of the phases observed in BSC images can then be evaluated and differentiation between sigma (σ) and chi (χ)-phases was possible considering that chi (χ)-phase is Mo-rich phase, when compared to sigma (σ) phase.

For EDS analysis, samples with high volume fraction of phases were selected. As an example, two different phases of the sample aged for 12 hours at 1023 K (750 °C), presented in Figure 5, were analyzed using EDS. The brighter phase identified as point (2) in Figure 5 is richer in Mo in relation to the light-gray phase, identified as (1), as presented in Table II and in the EDS spectra of Figure 6. Recent studies[8] reported the brighter phase as chi-phase due to its higher molybdenum levels if compared to sigma phase. For this reason, the lighter phase indicated in BSC micrographs was identified as chi. Sigma phase was identified as the light-gray phase of the BSC micrographs, since it

has high Cr and Mo contents, but smaller Mo contents than the phase identified as chi.

The longest aging times studied presented typical microstructures represented in Figure 7. Not only the increase in sigma volume fraction is prominent, but also the reduction or the absence of chi-phase. Some intergranular chi-phase are observed, particularly for the temperatures between 973 K and 1073 K (700 °C and 800 °C) (Figures 7(a) though (b)), probably associated to saturation of the heterogeneous nucleation sites in ferrite/ferrite and ferrite/austenite interfaces.

B. *Quantitative Analysis*

A computational thermodynamics simulation using Thermo-Calc© (TCFE8 database) was generated to predict equilibrium phase formation as a function of aging temperature (Figure 8). Chi-phase is not expected in equilibrium according to the simulation, indicating that the observed χ phase in Figures 2, 3, 4, and 7 will probably be transformed into another phase with the
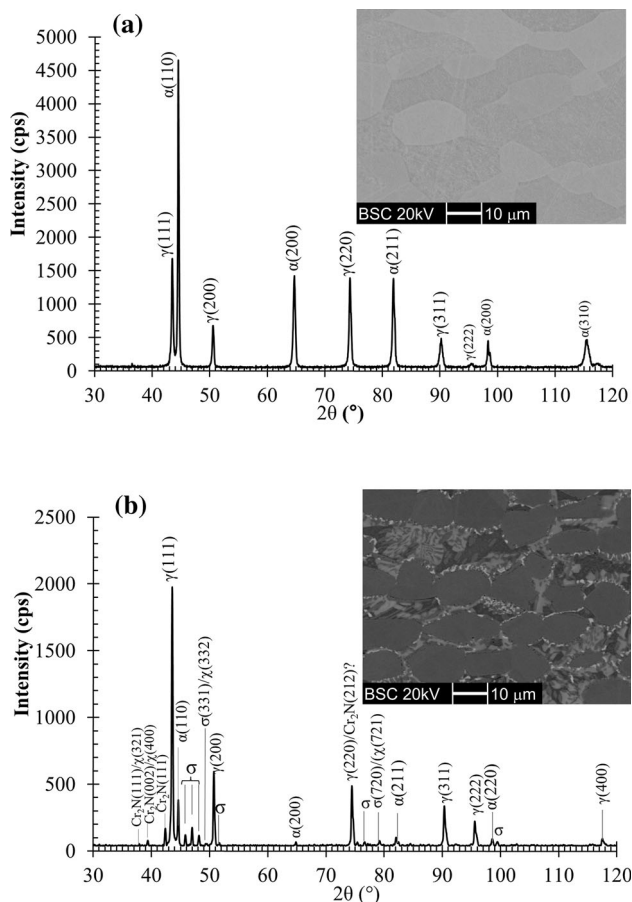
Fig. 3—X-ray diffraction patterns of UNS S31803 duplex stainless steel (*a*) solution-treated sample; (*b*) sample aged for 4 h at 973 K (700 °C). Typical BSC-SEM micrographs of both conditions are also presented.

progress of aging. In parallel to sigma formation, the thermodynamic simulation predicts the formation of chromium nitrides of Cr_2N type, which are actually observed close to the ferrite/ferrite and ferrite/austenite boundaries (Figures 2 through 4) and was detected in XRD patterns (Figure 3). Since nitrides are found in low volume fraction at all aging temperatures below 1123 K (850 °C), this phase was not considered in the transformation kinetic studies of this work.

The experimental sigma phase fraction for 360 hours at each studied aging temperature are plotted in Figure 8, for comparison between experimental and simulated data. It can be observed that between 973 K and 1073 K (700 °C and 800 °C) the equilibrium sigma volume fractions are close to the experimental measurements. Nevertheless, between 1073 K and 1223 K (800 °C and 950 °C), a deviation was registered between experimental and simulated sigma fractions, showing that simulation of equilibrium in this temperature range needs adjustments. However, this subject is out of the scope of this work, and it was mentioned for further reference for developments in this field of research.

The experimental values of the volume fractions of ferrite (obtained by ferritscope) are presented in Figure 9, while sigma and chi-phases (obtained through quantitative analysis from BSC images) are presented in Figures 10 and 11 respectively, both as a function of aging time in different temperatures. It is observed ferrite consumption together to the increase of sigma phase with increasing aging time, indicating that sigma is primarily formed from ferrite. There are also evidences of sigma formation from austenite in the end of the studied aging time between 1023 K and 1173 K (750 °C and 900 °C), since there is an increase in sigma phase fraction even in the absence of ferrite. Nevertheless, one cannot ignore the hypothesis of sigma phase formation from austenite during the aging treatment. This may occur because of the intense impoverishment in Cr and Mo of ferrite, leading to sigma formation from austenite.

For the temperatures of 973 K and 1223 K (700 °C and 950 °C), ferrite was not totally consumed due to sigma formation. The equilibrium simulation (Figure 8) predicts ferrite for the temperature of 1223 K (950 °C), but not for 1023 K (750 °C) suggesting that the equilibrium may not been reached until 360 hours of aging at 973 K (700 °C).

It is evident in Figure 11 the consumption of chi-phase after 6 hours of aging for the temperatures of 973 K and 1023 K (700 °C and 750 °C), which may be related to its transformation to sigma phase, increasing the total amount of this phase. As reported before, and according to the thermodynamic simulation, chi was not an equilibrium phase, which leads to the consumption of this phase with increasing aging time. For the temperatures of 973 K and 1073 K (700 °C and 800 °C), chi is not totally consumed, indicating again that equilibrium could not be reached until 360 hours of aging at those temperatures. It is worth noting that chi-phase was not observed between 1123 K and 1223 K (850 °C and 950 °C)

The kinetics of sigma phase formation was described here using the linearized Kolmogorov-Johnson-Mehl-Avrami (K-J-M-A) expression presented in Eq. [3]:

$$\ln[-\ln(1-f)] = n[\ln(t)] + \ln(k). \qquad [3]$$

Plots of $\ln[-\ln(1-f)]$ as a function of $[\ln t]$ are reported in Figure 12, allowing the determination of n and k for each aging temperature studied in this contribution.

A non-linearity of the data points in Figure 12 was observed for the aging between 973 K and 1173 K (700 °C and 900 °C) (Figures 12(a) through (e)), suggesting a double stage in sigma phase formation. This provide two K-J-M-A exponent (n) and constant (k) for each temperature, related to the two slopes found in Figure 12, as reported in Table III, in accordance to the works previously mentioned.[7,17]

It is evident that the aging temperature of 1223 K (950 °C) presents a different kinetic behavior than the other temperatures (Figure 12(f)). Probably this is related to the different morphologies observed at different aging temperatures: a more compact morphology is observed at 1223 K (950 °C) both in the earlier stages of sigma formation (Figure 4(d)) and in the longest aging
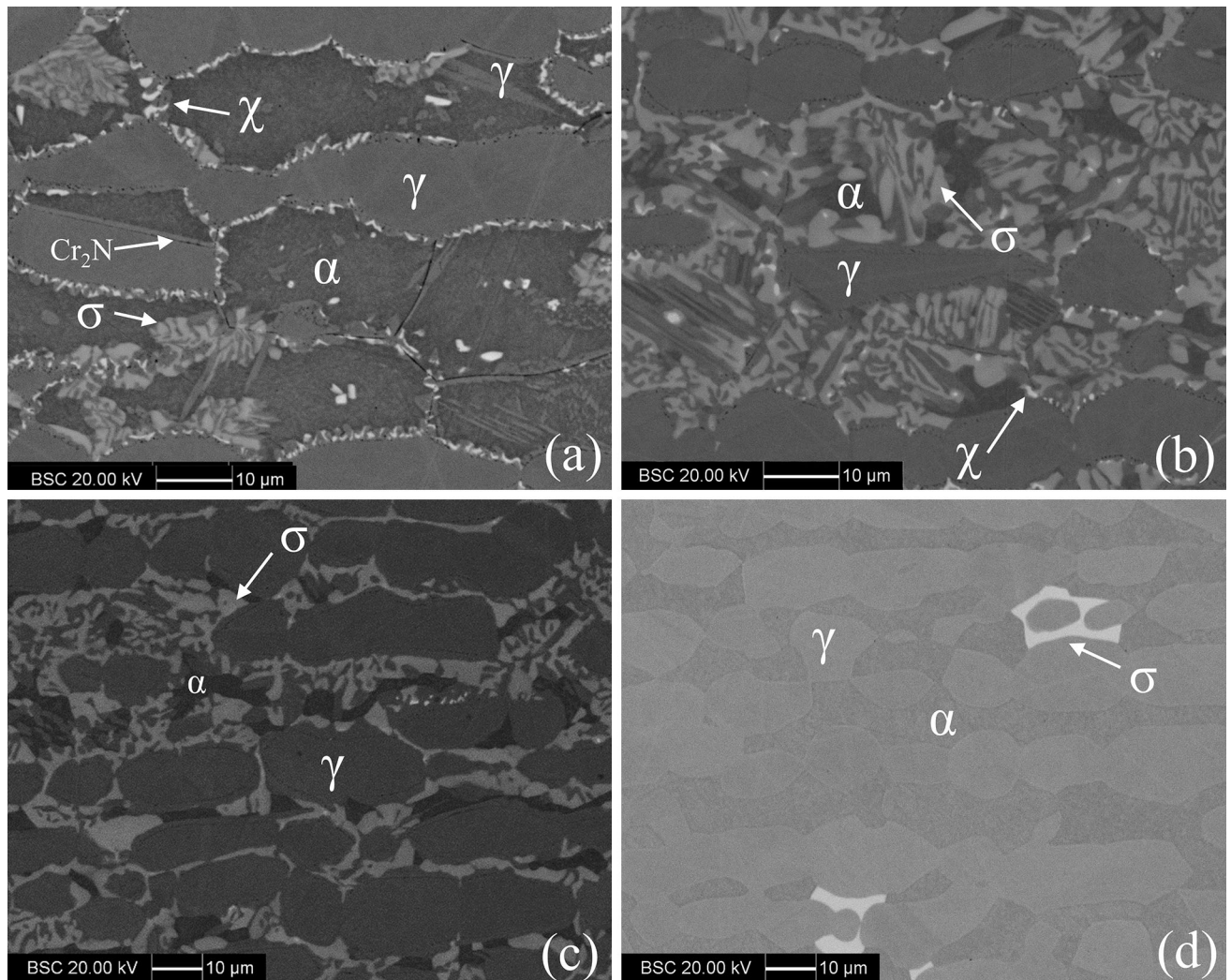
Fig. 4—Microstructures of UNS S31803 aged for 4 h at: (*a*) 1023 K (750 °C); (*b*) 1073 K (800 °C); (*c*) 1173 K (900 °C); and (*d*) 1223 K (950 °C).
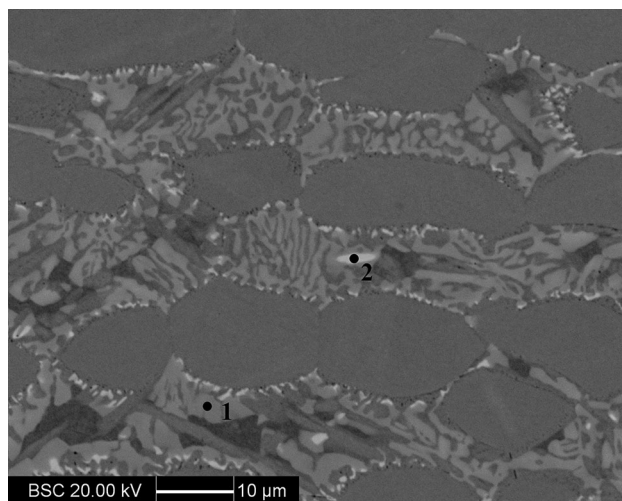

Fig. 5—Identification of areas analyzed by EDS in UNS S31803 sample aged for 12 h at 1023 K (750 °C).

time analyzed (Figure 7(d)). On contrast, a lamellar morphology is observed in lower temperatures (Figures 4(a) through (c)), remaining lamellar even in the possibility of sigma coarsening (Figures 7(a) and (b)). Coarsening of sigma phase, however, is promoted by the longer aging times (Figures 7(b) and (c)), or the higher aging temperatures, 1173 K to 1223 K (900 °C to 950 °C).

Values of the K-J-M-A exponent for all temperatures studied in this research were compared to the values established in literature.[19] It was found that the first slope in K-J-M-A plots (Figures 12(a) through (e) and Table III) can be related to nucleation and growth controlled by interface (*n* ~1 to 4), while the second slope is related to diffusional-controlled growth (*n* ~0 to 0.5).

The *n* values found in this contribution are different from the values reported by Elmer *et al.*[17] that have found *n* = 7 for the first stages of sigma formation and *n* = 0.75 for the final stages. In addition, Magnabosco[11] in a previous work found a different

Table II. EDS Analysis of the Sample Aged for 12 h at 1023 K (750 °C)

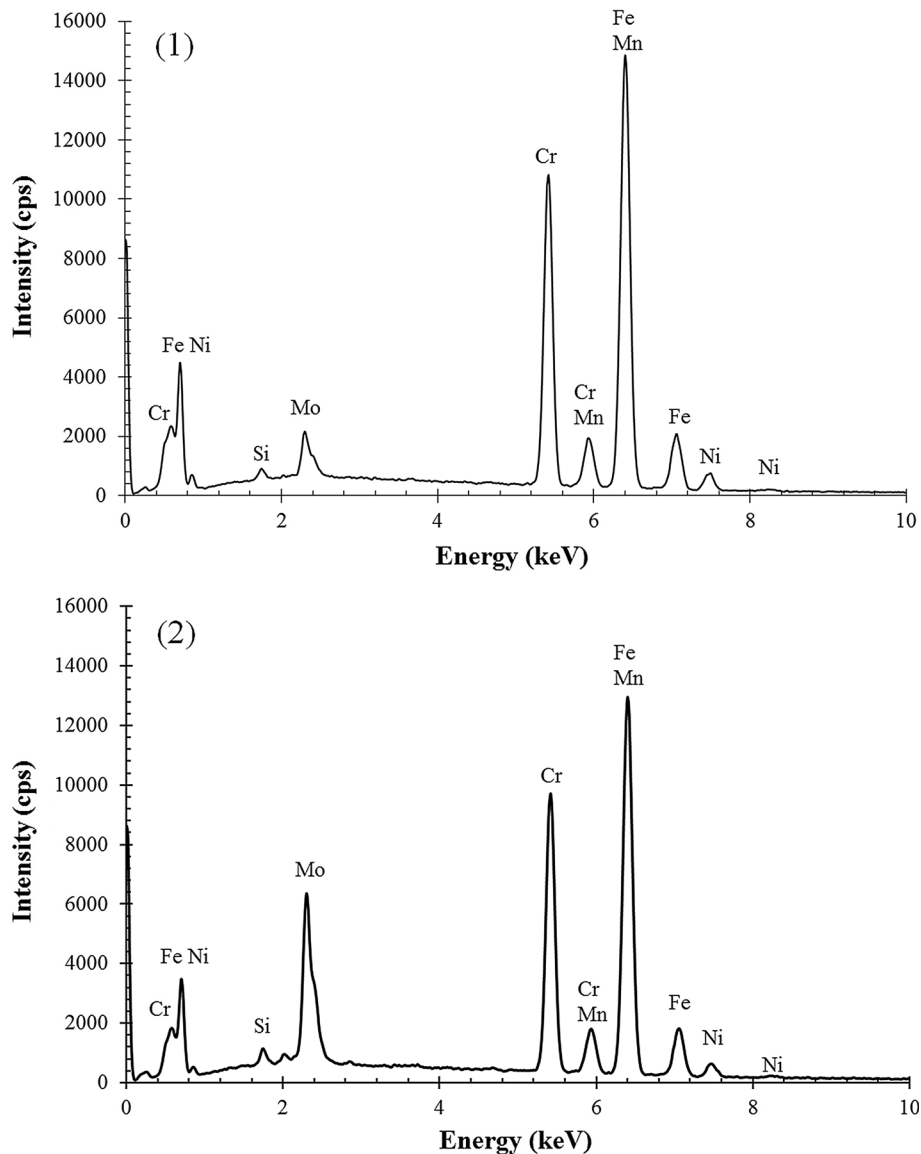|	Cr (wt pct)	Ni (wt pct)	Mo (wt pct)	Si (wt pct)	Mn (wt pct)
(1)	17.58 ± 0.23	2.87 ± 0.12	17.58 ± 0.23	0.71 ± 0.05	1.43 ± 0.10
(2)	27.84 ± 0.18	3.86 ± 0.13	5.01 ± 0.18	0.51 ± 0.05	1.46 ± 0.11

Fig. 6—EDS spectra for the selected areas indicated in Fig. 5.

kinetic behavior showing just one slope in K-J-M-A plots ($n = 0.915 \pm 0.144$). The differences found may be related to the solution-treatment conditions used in each work: 2.5 hours at 1338 K (1065 °C)[17] and 30 minutes at 1393 K (1120 °C), respectively,[11] both different from the solution-treatment conditions employed in this work, 30 minutes at 1448 K (1175 °C). Different solution treatment conditions leads to different ferrite and austenite fractions and chemical compositions, and different grain sizes, generating different conditions for heterogeneous nucleation and growth of the intermetallic phases.

The hypothesis of different govern stages in sigma formation, associated to nucleation in the first slope and growth coarsening in the second slope, is confirmed by the microstructural characterization presented here. Even in the lowest aging temperature studied, 973 K (700 °C), a distinction between a nucleation governed stage (Figure 13(a)) and a growth-coarsening stage (Figure 13(b)) can be observed. Only at 1223 K (950 °C)
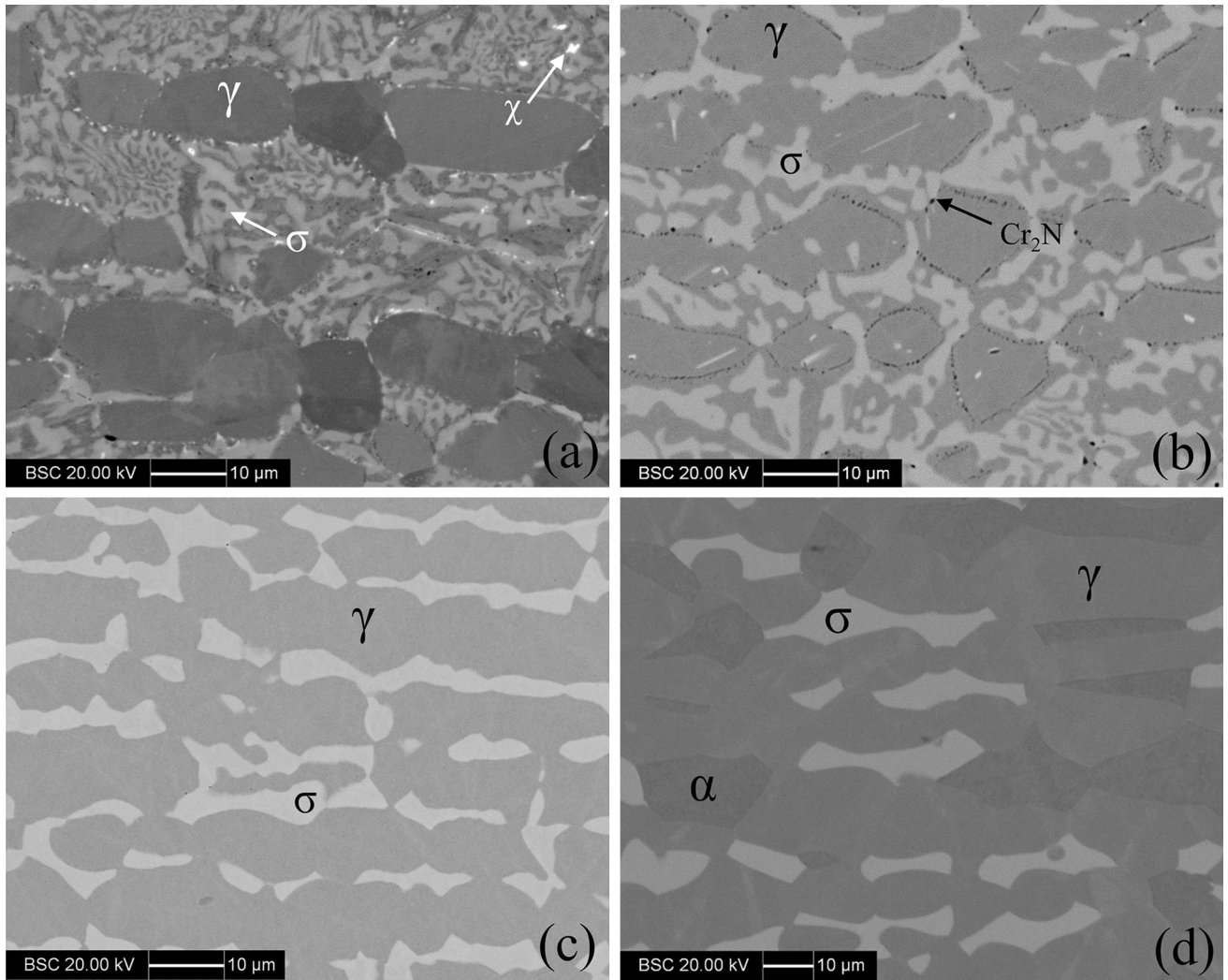
Fig. 7—Microstructures of UNS S31803 aged for 360 h at: (*a*) 973 K (700 °C); (*b*) 1073 K (800 °C); (*c*) 1173 K (900 °C); (*d*) 1223 K (950 °C).
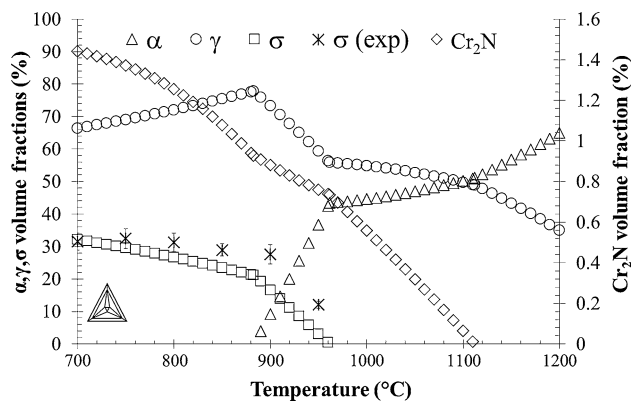

Fig. 8—Thermo-Calc© TCFE8 simulation of phases volume fractions of studied UNS S31803 duplex stainless steel, and sigma phase volume fractions after 360 h of aging, σ (exp), as a function of temperature.
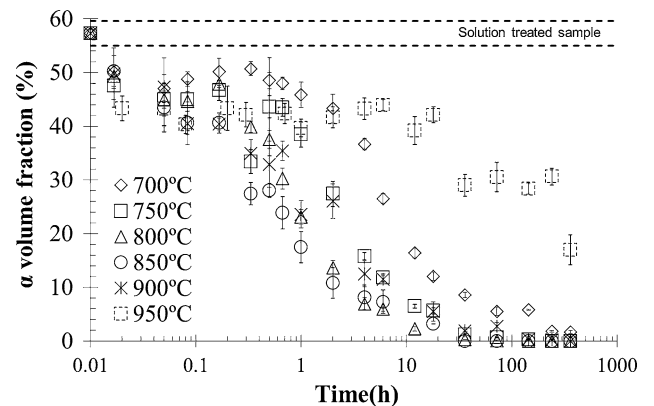
Fig. 9—Ferrite volume fraction obtained by ferritscope as a function of aging time of UNS S31803 duplex stainless steel.

this microstructural observation was not possible, confirming that only the growth coarsening of individual particles of sigma is the govern stage at this temperature.

During the first stage of sigma formation at 973 K (700 °C), n values reaching 4 was observed, which is, in accordance to the literature,[19] related to the growth of sigma phase in 3 directions, since in the early stages of
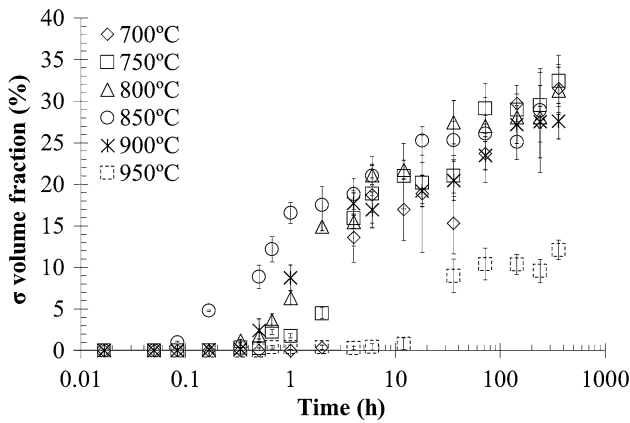
Fig. 10—Volume fraction of sigma obtained by BSC image quantitative analysis as a function of aging time of UNS S31803 duplex stainless steel.
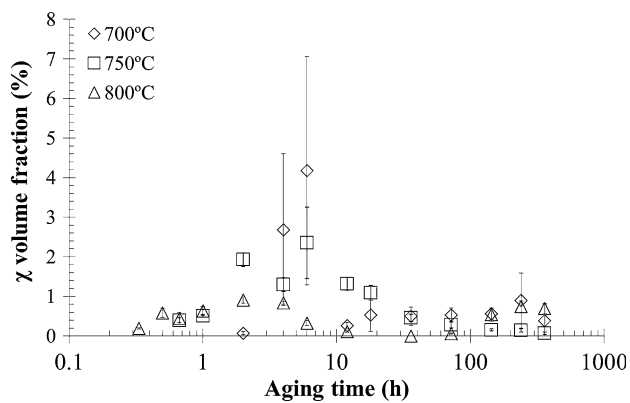

Fig. 11—Volume fraction of chi obtained by BSC image quantitative analysis as a function of aging time of UNS S31803 duplex stainless steel.

Table III. K-J-M-A Exponent (*n*) and Constant (*k*) in the Two Different Slopes of Fig. 12 for UNS S31803 Duplex Stainless Steel Aged Between 973 K and 1223 K (700 °C and 950 °C)

	n		*k*	
T [K (°C)]	1st Slope	2nd Slope	1st Slope	2nd Slope
973 K (700 °C)	3.9329	0.3176	0.0007	0.4248
1023 K (750 °C)	1.5898	0.3159	0.0595	0.4479
1073 K (800 °C)	2.4557	0.2853	0.2247	0.5716
1123 K (850 °C)	1.4227	0.2236	0.4314	0.7291
1173 K (900 °C)	1.8949	0.4599	0.1400	0.3834
1223 K (950 °C)	0.9449	—	0.0185	—

sigma formation, there are no preferential growing direction in identified sigma particles (Figure 2(a)). With increasing aging time, sigma evolves to discontinuous, lamellar morphology (Figure 2(b)), with preferential growth in two directions (*n* ~ 3).

For temperatures between 1023 K and 1173 K (750 °C and 900 °C), the initial slopes show the

nucleation of sigma mainly in the triple points (*n* ~ 2) or grain boundaries (*n* ~ 1), as exemplified in Figures 4(a) through (c). Both mechanisms are interface controlled. According to Avrami theory,[13,14] the *n* value between 1 and 2 are related to the preferential growth in one or two directions which explain the lamellar morphology presented for example in Figures 4(a) through (c).

Values of *n* in the second slope (*n* ~ 0.5) of the aging at 973 K (700 °C) can be related to sigma growth by plates thickening, which is confirmed by sigma coarsening as observed in Figures 2(c) and (d) and in Figure 13. In the second slope, all K-J-M-A exponents are smaller than unity, which means that all the growth conditions occur with no preferential direction and are probably related to the coarsening of sigma, what is evident when comparing Figures 2, 4, and 7.

The stage governed by nucleation of sigma, characteristic of the first slope, is replaced by the growth-coarsening governed stage, characterized by the second slope. It can be then stated that exist a transition of the kinetic mechanism of sigma formation.

The transition times of kinetic mechanisms of sigma phase formation for each temperature studied in this research, previously indicated by the intersection between the first and the second slope in Figure 12, are represented in Figure 14. It can be concluded that the increase of aging temperature leads to the reduction of the required time do change the controlling stage of sigma phase formation from nucleation governed to diffusion-controlled growth coarsening. This behavior is related to the increase of the diffusion rates of the elements (such as Cr and Mo) from which sigma is composed.

Using the K-J-M-A constant *k*, the activation energy for sigma phase formation in both stages can be estimated. For that, the linearized form of Eq. [2] was used (Eq. [4]):

$$\ln k = \ln k_0 - \frac{Q_\sigma}{R \cdot T}. \qquad [4]$$

From Eq. [4] and plotting ln *k* as a function of reciprocal temperature (Figure 15), it was possible to evaluate the activation energy of sigma phase formation between 973 K and 1123 K (700 °C and 850 °C) for the two controlling stages of sigma phase formation: nucleation governed (first slope) and diffusion-controlled growth coarsening (second slope). Due to the low correlation in the linearization of K-J-M-A model for 1173 K (900 °C), this temperature was excluded of the mentioned analysis. This temperature can also be considered as a landmark between the two governed stages of sigma formation, which clearly occurs in the temperature range of 973 K to 1123 K (700 °C to 850 °C)—Figures 12(a) through (d)—and the one governed stage sigma formation, which occurs at 1223 K (950 °C), represented by Figure 12(f).

Contrary to what some authors[15] claims, that it is not possible to determinate the activation energy of sigma phase formation because of the change in the mechanism of formation, which leads to a double slope, the activation energy for nucleation governed and
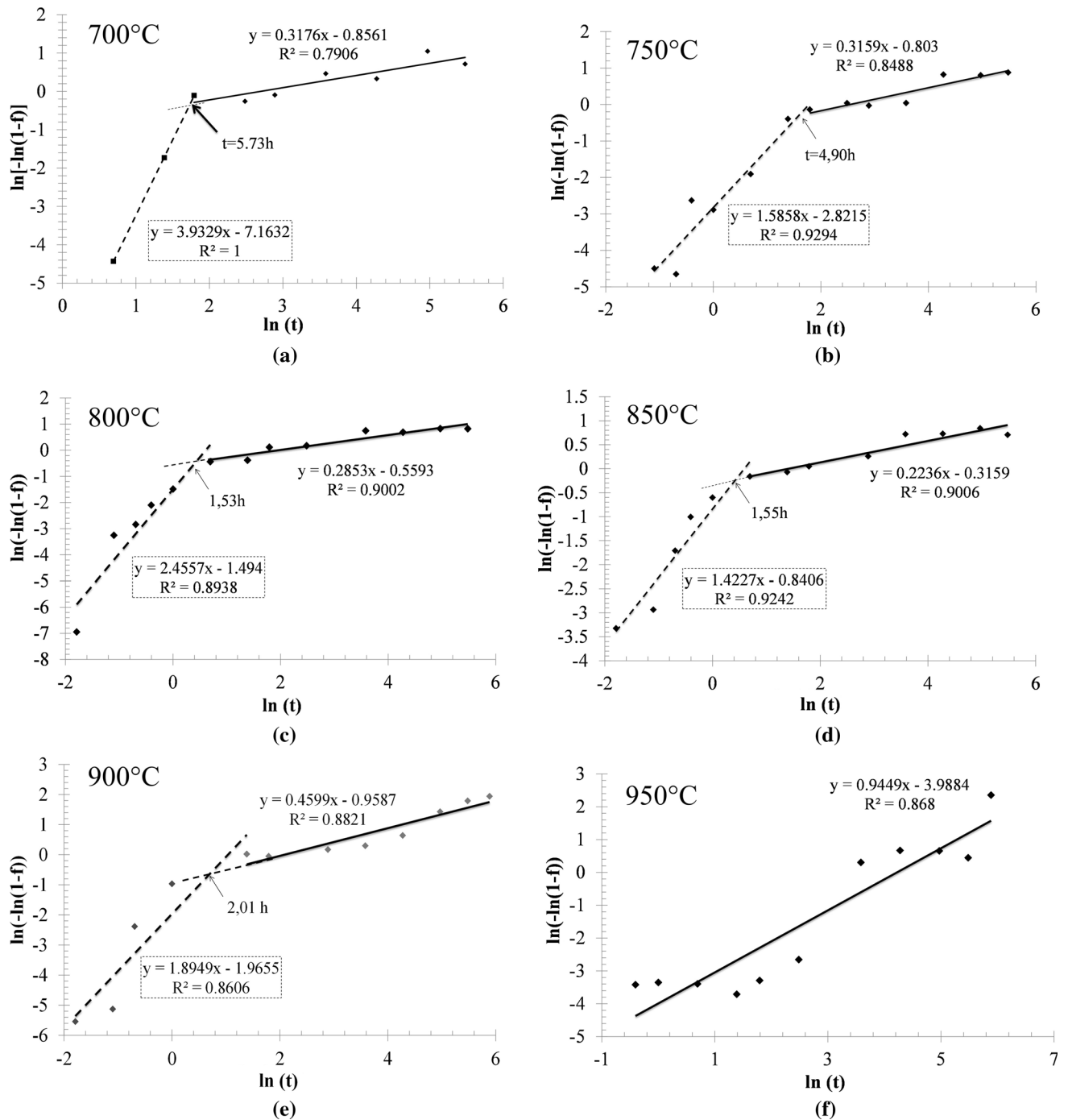
Fig. 12—Linearized sigma volume fraction as a function of time assuming Kolmogorov-Johnson-Mehl-Avrami (K-J-M-A) kinetic model for sigma phase formation in UNS S31803 duplex stainless steel: (a) 973 K (700 °C); (b) 1023 K (750 °C); (c) 1073 K (800 °C); (d) 1123 K (850 °C); (e) 1173 K (900 °C); (f) 1223 K (950 °C). Where a transition between two slopes were observed, the transition times are marked.

diffusion-controlled growth coarsening of sigma phase could be estimated, respectively, as 341 and 24 kJ mol^{-1}.

As discussed before, if the first slope is related to the nucleation, and the second slope to the growth/coarsening of sigma phase, higher activation energy is required to the nucleation of this phase. As the nucleation process decreases its importance, the growth occurs more easily, requiring lower energy. In addition, both activation energy for nucleation and growth are higher than the required activation energy for chromium diffusion in ferrite (235 ± 15 kJ mol^{-1}) and austenite (278 ± 15 kJ mol^{-1}) reported in literature.[11] Nevertheless, the estimated activation energies to sigma phase formation are close to the values reported for molybdenum diffusion in ferrite (289 ± 13 kJ mol^{-1}).[22] This information allows the hypothesis that the diffusion of Mo controls the nucleation of sigma phase.
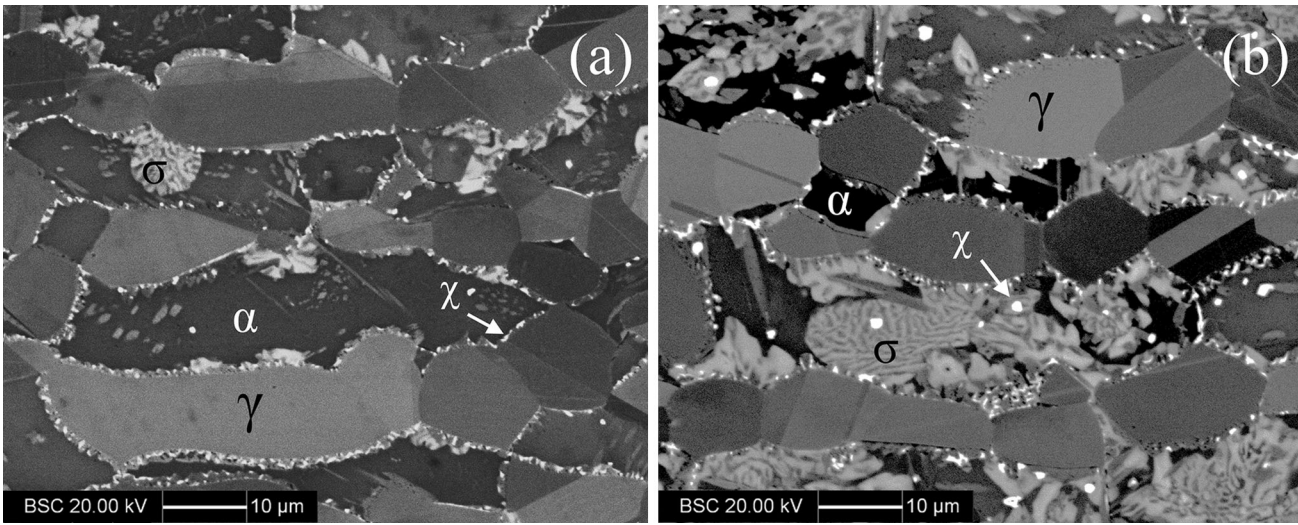
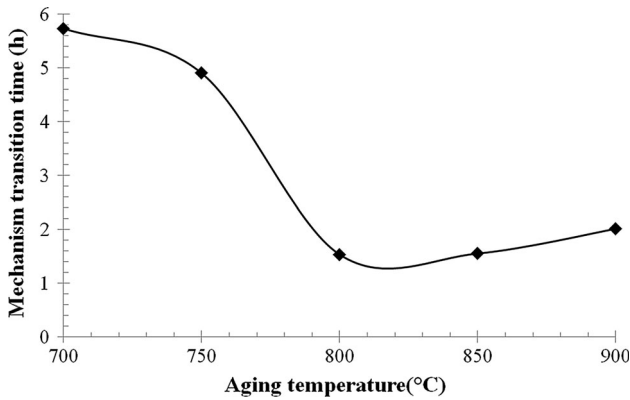Fig. 13—Microstructural evolution of UNS S31803 duplex stainless steel aged at 973 K (700 °C) for: (*a*) 4 h (*b*) 12 h.

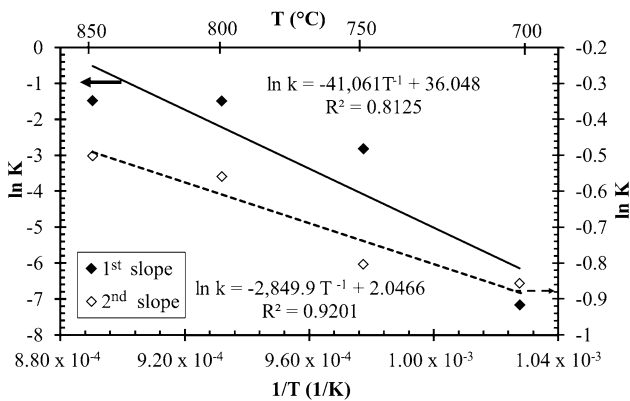Fig. 14—Kinetic mechanism transition time as a function of aging temperature.
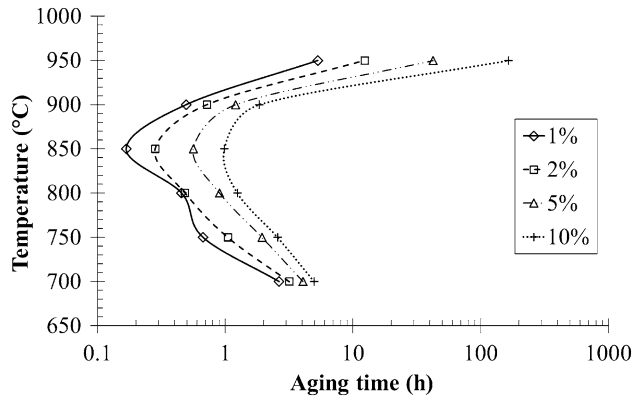

Fig. 16—Time-Temperature-Transformation diagram for sigma phase formation in UNS S31803 aged between 973 K and 1223 K (700 °C and 950 °C).

Fig. 15—ln *k* as a function of reciprocal temperature of aging.

The pre-exponential constants (k_0) were also estimated in 4.5×10^{15} for the first slope, and 7.74 for the second slope. It is possible to predict the sigma volume fraction as a function of aging through Eq. [5]:

$$\text{pct}\sigma = \text{pct}\sigma_{\text{eq}} \cdot \left[1 - e^{-kt^n} \right], \qquad [5]$$

where pct σ_{eq} correspond to the equilibrium sigma volume fraction, considered to be the measured sigma volume fraction at the end of the aging (360 hours).

From Eq. [5], the time–temperature-transformation (TTT) diagram for sigma phase formation was generated (Figure 16) where the "*c* curves" characteristic of nucleation and growth mechanisms are observed. The high kinetic of sigma phase formation occurs at 1123 K (850 °C), as reported by previous authors.[1–5,9,11,12]

It is important to highlight that for the sigma volume fraction of 1 pct, a "double c curve" is evident in Figure 16. The lower temperature "*c* curve" is probably influenced by chi-phase formation. Occurring primarily between 973 K and 1073 K (700 °C and 800 °C) (Figure 11), chi-phase may be act as a heterogeneous nucleation site for sigma phase formation, in a temperature range where Mo diffusion, supposed as the controlled step in sigma nucleation, is slower than in higher temperatures. The higher temperature "*c*" curve takes place in a range of temperature that Mo diffusion is easier, allowing the nucleation of sigma phase without

the help of the heterogeneous nucleation sites provided by chi-phase.

IV. CONCLUSIONS

1. The kinetic study of sigma phase formation using K-J-M-A model shows a change in the main mechanism of sigma formation aged between 973 K and 1173 K (700 °C and 900 °C), from a nucleation-governed stage to a diffusion-controlled growth-coarsening stage, confirmed by a double inclination in K-J-M-A plots and microstructural observations.
2. A single inclination in K-J-M-A plots was observed for the 1223 K (950 °C) aging temperature showing that kinetic behavior in this temperature is only related to diffusion-controlled growth of sigma phase.
3. The activation energy for nucleation of sigma phase estimated by the proposed kinetic study is higher than the activation energy for its growth. This is an evidence of when sigma is nucleated, its growth occurs more easily because of the high diffusion rates afforded by high aging temperatures.
4. The estimated activation energies for the nucleation of sigma phase are close to the molybdenum diffusion in ferrite showing that probably the diffusion of molybdenum controls the nucleation of sigma phase.
5. The proposed time-temperature-transformation (TTT) diagram shows a "double c curve" configuration, probably associated to the presence of chi-phase formed between 973 K and 1073 K (700 °C and 800 °C), which acts as heterogeneous nuclei for sigma phase formation in lower aging temperatures.

ACKNOWLEDGMENTS

REFERENCES

1. J. Charles: *Rev. Met.*, 2008, vol. 105, pp. 155–71.
2. J.O. Nilsson: *Mater. Sci. Technol.*, 1992, vol. 8, pp. 685–700.
3. H.D. Solomon and T.M.J. Devine: *ASM Metals Park*, 1982, pp. 693–756.
4. E.O. Hall and S.H. Algie: *Metal. Rev.*, 1966, vol. 11, pp. 61–88.
5. K.H. Lo, C.H. Shek, and J.K.L. Lai: *Mater. Sci. Eng.*, 2009, vol. 65, pp. 39–104.
6. R. Magnabosco and N. Alonso-Falleiros: *Corrosion*, 2005, vol. 61, pp. 130–36.
7. D.C. Dos Santos and R. Magnabosco: *Corrosion*, 2013, vol. 69, pp. 900–11.
8. Z. Zhang, H. Zhao, H. Zhang, Z. Yu, J. Hu, L. He, and J. Li: *Corros. Sci.*, 2015, vol. 23, pp. 120–25.
9. K.H. Lo, C.T. Kwok, and W.K. Chan: *Corros. Sci.*, 2011, vol. 53, pp. 3697–3703.
10. D.M. Escriba, E. Materna-Morris, R.L. Plaut, and A.F. Padilha: *Mater. Charact.*, 2009, vol. 60, pp. 1214–19.
11. R. Magnabosco: *Mater. Res.*, 2009, vol. 12, pp. 231–37.
12. M. Pohl, O. Storz, and T. Glogowski: *Mater. Charact.*, 2007, vol. 58, pp. 65–71.
13. M. Avrami: *J. Chem. Phys.*, 1939, vol. 7, pp. 1103–12.
14. M. Avrami: *J. Chem. Phys.*, 1940, vol. 8, pp. 212–24.
15. W. Johnson and R. Mehl: *Trans. AIME*, 1939, vol. 135, pp. 416–41.
16. A. Kolmogorov: *Akad. Nauk SSSR, Izv. Ser. Mat.*, 1937, vol. 1, pp. 355–59.
17. J.W. Elmer, T.A. Palmer, and E.D. Specht: *Metall. Mater. Trans. A*, 2007, vol. 38A, pp. 464–75.
18. P. Ferro and F. Bonollo: *Metall. Mater. Trans. A*, 2012, vol. 43A, pp. 1109–2012.
19. J.W. Christian: *The Theory of Transformations in Metals and Alloys*, 2nd ed., Pergamon, Oxford, 2002, pp. 529–52.
20. J. Goldstein, DE Newbury, D.C. Joy, C.E. Lyman, P. Echlin, E. Lifshin, L. Sawyer, and J.R. Michael: *Scanning Electron Microscopy and X-ray Microanalysis*, 3rd ed., Springer, New York, 2003, pp. 77–79.
21. V.T. Borisov, V.M. Golikov, and G.V. Sherbendindkiy: *Fizik. Metallov. Metall.*, 1966, vol. 22, pp. 175–76.
22. H. Nitta and K. Miura: Y. IIjima*Acta Mater.*, 2006, vol. 54, pp. 2833–47.